

Correlation Between Vortex Ring Formation and Mitral Annulus Dynamics During Ventricular Rapid Filling

ARASH KHERADVAR,*† MICHELE MILANO,† AND MORTEZA GHARIB*†

One of the most important fluid phenomena observed in the left ventricle during diastole is the presence of vortex rings that develop with a strong jet entering through the mitral valve. The present study is focused on the rapid filling phase of diastole, during which the left ventricle expands and receives blood through the fully open mitral valve. The atrioventricular system during the rapid filling phase was emulated experimentally with a simplified mechanical model in which the relevant pressure decay and the dimension of mitral annulus approximate the physiologic and pathologic values. Digital particle image velocimetry measurements were correlated with the force measurements on the mitral annulus plane to analyze the relation between flow and the mitral annulus motion. The recoil force on the displaced annulus plane was computed on the basis of plane acceleration and plane velocity and correlated with the inflow jet. Measurements of the recoil force for different values of the mitral annulus diameter showed that the recoil force was generated during fluid propulsion and that it is maximal for an annulus diameter close to the normal adult value in a healthy left ventricle. We also tested annulus diameters smaller and larger than the normal one. The smaller annulus corresponds to the stenotic valves and the larger annulus exists in dilated cardiomyopathy cases. In both conditions, the recoil force was found to be smaller than in the normal case. These observations are consistent with the previously reported results for dilated cardiomyopathy and mitral stenosis clinical conditions. *ASAIO Journal* 2007; 53:8-16.

The topic of vortex rings has received much attention over the past few years. Vortex rings occur in nature wherever propulsive flow exists, from erupting volcanoes to the ones generated by squid and jellyfish to propel them. They are also present in the left ventricle (LV). The current understanding of the formation process and dynamics of the vortex rings has been extensively described in the literature.¹⁻⁴ However, the

process of vortex ring formation and its influence on dynamics of the left heart have not been elucidated so far.

The presence of vortex rings that develop during cardiac diastole was initially recognized by *in vitro* visualization of the ventricular flow^{5,6} and subsequently confirmed by analyses based on color Doppler mapping^{7,8} and magnetic resonance imaging.^{9,10} During diastole, when the left ventricle is filling with the blood jet from the atrium, the ventricle expands, and as a result, the atrioventricular plane moves in the opposite direction with respect to blood flow. Little has been done so far to understand if any correlation exists between this movement and the formation process of the vortex ring created by the blood jet.

Vortex rings typically develop from a jet or slug of fluid ejected from a nozzle. In fluid mechanics, mitral inflow is considered a starting jet ejected from left atrium to the left ventricle. The characteristic stroke ratio of a starting jet (L/D), typically produced by a piston-cylinder mechanism, is identified as the ratio of the ejected jet length ($L = \int_T u_{piston}(t) dt$; where u_{piston} is the piston velocity, t is time, and T is the period of piston displacement) to the effective jet diameter (D). This ratio is usually referred to as "formation time"^{3,11,12} and is a nondimensional measure of time. Gharib *et al.*³ discovered that by increasing the stroke ratio of a starting jet to values >4 , in semi-infinite space, no additional energy or circulation enters the leading vortex ring and the remaining fluid in the pulse will be ejected as a trailing jet. After this stage, the vortex ring is said to have pinched off from the starting jet, and as a result, the size of the leading vortex ring cannot increase. The value of the stroke ratio (formation time) at which pinch-off occurs is recognized as vortex formation number. Gharib *et al.*³ experimentally showed that regardless of the jet velocity and the nozzle size, in a semi-infinite space, the formation number lies between 3.6 and 4.5.

In a different experimental study, Krueger and Gharib¹³ showed that the time-averaged thrust generated by a pulsed jet in semi-infinite space would be maximized once a vortex ring with maximum circulation is created. In other words, once the stroke ratio of a pulsed jet is large enough to pinch off the leading vortex ring and initiate formation of the trailing jet flow, further increase in stroke ratio does not increase the time-averaged thrust. Krueger and Gharib¹³ emphasized that formation of a single leading vortex ring has a more significant role in efficient generation of thrust when compared with the trailing jet.

In the present article, we studied the formation of a vortex ring in a confined chamber in contrast to previous studies done in a semi-infinite space. The objective was to understand the dynamics of mitral annulus plane and its correlation with

From the *Cardiovascular and Biofluid Dynamics Laboratory, California Institute of Technology, Pasadena, California; and the †Graduate Aeronautical Laboratory, California Institute of Technology, Pasadena, California.

Submitted for consideration May 2006; accepted for publication in revised form July 2006.

Reprint requests: Dr. Arash Kheradvar, Mail Code 301-46, California Institute of Technology, 1200 East California Boulevard, Pasadena, CA 91125.

DOI: 10.1097/01.mat.0000249870.44625.22

transmitral flow by using vortex ring formation as an index. To study this, we chose a simplified system to experimentally simulate the contribution of a vortex ring on dynamics of the annulus plane.

In a normal ventricle, the annulus plane motion is mainly a consequence of compliance effect and passive stiffness of myocardium. However, the compliant walls of the ventricle would affect generation of a vortex ring along with the transmitral jet by dropping the LV pressure (suction effect) during diastole¹⁴ and would literally interact with the formed vortex.¹⁵ As a result, we chose to generate a vortex ring by using an exponential pressure drop, mimicking the suction in the LV^{16–18} while carefully avoiding the influence of other factors.

In this study, the annulus is circular in shape, whereas the mitral annulus is oval-shaped and contains leaflet structures that interact with the flow. However, incorporating leaflets without knowing the behavior of the system without the valve makes the interpretation of results more difficult. Since no valve is used in this study, we only consider the effect of suction on generating jet once the mitral valve is fully open.

Methods

The experimental setup was a simplified analog of the left heart during the rapid filling phase of diastole. In early diastole, pressure decays fast in the LV, the mitral valve opens immediately in response to pressure drop, allowing blood transfer from atrium to ventricle, and finally, the valve plane moves in the opposite direction with respect to the blood flow. To be consistent with cardiac physiology, the LV pressure drop in early diastole was modeled as a decaying exponential function with physiologic pressure drop time constant.¹⁶

Experimental Setup Components

The experimental setup was composed of two chambers partially filled with water; the nominal ventricle was built as a Plexiglas chamber connected to a suction pump (VSI SPS3891, Vivitro Systems Inc., Victoria, BC, Canada) to generate pressure drop, and the nominal atrium was a cylindrical tube sitting inside the ventricular chamber as shown in **Figure 1**. Dimensions of the ventricular box were 13 cm (width) by 13 cm (depth) by 20 cm (height), though only the lower 13 cm of the box was filled with fluid (**Figure 1**). The base (annulus plane)–apex distance was set to 9 cm, which is the same as the base–apex distance in LV, as mentioned in medical literature.^{19,20} The fully open mitral annulus was experimentally simulated as a flat plate with a circular annulus, which was made of neutrally buoyant Plexiglas to avoid any behavior influenced by difference in density. Additionally, to prevent the effect of mass transfer on annulus-plane dynamics, a low flow–resistant pneumatic check valve (R-702, Resenex Corp., Chatsworth, CA) was placed on the ventricular chamber. The mass of the fluid entering from the atrial tube pushed the trapped air into the ventricular chamber to leave the box through the check valve, avoiding the mass transfer effect.

To reproduce the movement of the valve plane during early diastole, the annulus plane was allowed to slide into the downstream end of the atrial tube without friction. Three L-shaped rods prevented the plate from falling into the ven-

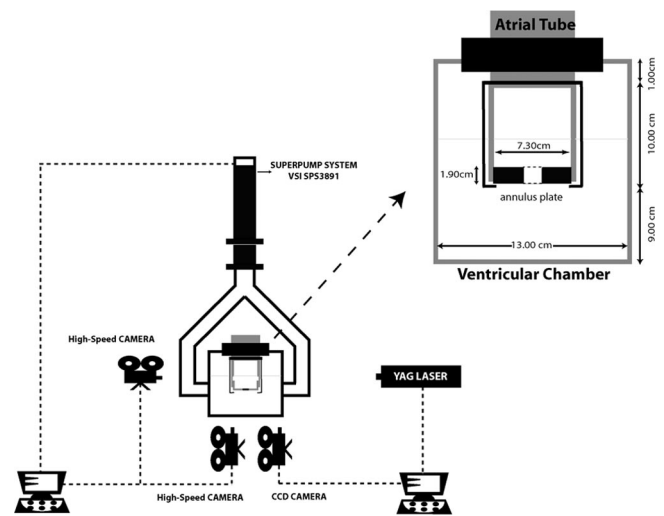


Figure 1. Schematics of the experimental setup. The experimental setup was composed of two chambers partially filled with water; the nominal ventricle was built as a Plexiglas chamber connected to a suction pump to generate pressure drop, and the nominal atrium was a cylindrical tube sitting inside the ventricular chamber as shown. Dimensions of the ventricular box were 13 cm (width) by 13 cm (depth) by 20 cm (height), though only the lower 13 cm of the box is full. The base (annulus plane)–apex distance was set to 9 cm. Two high-speed cameras track the water level velocity and the annulus plane motion. Flow was illuminated by a 25-mJ, double-pulsed Nd:YAG laser with pulse separation of 1 ms. A high-resolution monochrome CCD digital camera was positioned perpendicular to the ventricular chamber to capture the image sequences of particle field.

tricular chamber. The LV pressure drop was reproduced by using a computer-controlled suction pump. The considered range for pressure drop time constant was within the physiologic limits,^{21,22} and the volume of ejected fluid was set to 50 ml, which is equivalent to the volume of blood transferred into the human LV during early diastole.²³ Both chambers and the sliding annulus plane were constructed of Plexiglas to facilitate flow visualization and annulus plane motion measurements.

Reproduction of Early Diastole

For each experiment, both atrial and ventricular chambers were set to have atmospheric pressure. To reproduce the sudden pressure drop in early diastole, the suction pump created a rapid pressure difference between the water inside the cylindrical atrium and the water inside the ventricular chamber. Three different sizes for annulus diameter were used to experimentally simulate different flow conditions. For all the considered cases, the pump was set to displace a constant volume of fluid (50 ml) while the pressure drop scheme and the initial water height in the system were kept the same. The pressure inside the ventricular chamber and transannulus pressure were measured with a real-time pressure monitoring system during the experiment (Deltran DPT-400 pressure transducers, Utah Medical Products Inc., Midvale, UT, and VSI-TP8891, Vivitro Systems Inc., Victoria, BC, Canada). For accuracy of measurement and to make sure that the obtained results were reproducible and consistent with each other, every set of experiments was run in 20 consecutive cycles. For each single cycle,

the LV pressure was forced to decay as an exponential function in response to the applied suction:

$$P_{LV} = P_0 \exp\left(\frac{-t}{\tau}\right) \quad (1)$$

where P_0 is the initial pressure set to atmospheric value, τ is the pressure drop time constant and adjusted to be 35 ± 5 ms, and t is time. The duration of each cycle was set to 100 ms,^{24–26} imitating the duration of the rapid filling phase of diastole (E wave).

Measurement Methods

The displacement of the water level inside the atrial tube was captured by using a high-speed camera (Photron FAST-CAM-Ultima APX, Photron USA, Inc., San Diego, CA) at 250 frames per second. The water level velocity was computed by finite difference, based on the measured water level displacement data. Applying the continuity equation and considering a uniform profile for exit jet velocity over the annulus cross section, transannulus flow rate was computed as:

$$\frac{dV}{dt} = \frac{\pi}{4} D_A^2 \cdot (U_A - U_p) = \frac{\pi}{4} D_J^2 (U_J - U_p) \quad (2)$$

where V is the volume of fluid going through the annulus, U_J is the instantaneous exit jet velocity, U_A is the water level velocity at the atrium, U_p is the annulus plane velocity, and D_J and D_A are the annulus diameter and the cross-sectional diameter of the atrial tube, respectively. Instantaneous exit jet velocity (U_J) was computed as:

$$U_J(t) = \frac{D_A^2}{D_J^2} U_A(t) + \left(1 - \frac{D_A^2}{D_J^2}\right) U_p(t) \quad (3)$$

Displacement of the annulus plane was monitored by a second high-speed camera (same as the first camera mentioned earlier). The two cameras were synchronized to capture immediate changes in flow and the annulus plane dynamics. The mass of fluid inside the atrial tube at each instant of time was computed as:

$$\rho \int_{V_0}^{V_A(t)} dV_A = \rho \left(V_0 - \frac{\pi}{4} D_A^2 (x_0 - \int_{x_0}^{x(t)} dx) \right) \quad (4)$$

where ρ is water density, dV_A is the fluid volume element, V_0 is the initial volume of fluid in the atrium, x_0 is the initial position of atrial water level with respect to the origin before starting the experiment, $x(t)$ is the instant position of water level, and dx is atrial water level displacement element. Formation time (T^*) was computed on the basis of the definition described by Gharib *et al.*³ as:

$$T^* = \frac{1}{D_J} \int_0^t U_J(\xi) d\xi \quad (5)$$

The flow characteristic information (e.g., velocity field and circulation) was captured by phase-averaged digital particle image velocimetry (DPIV).²⁷ DPIV uses two digital images of a particle-seeded flow illuminated by a thin laser sheet to determine the displacement field of the particles in the field of view

(sampling window) by cross-correlating pixels in a subsection of two images. A high-resolution monochrome CCD digital camera (30 fps, 768×480 ; TM-9701, PULNIX America, Inc.) was positioned perpendicular to the ventricular chamber to capture the image sequences of the particle field (**Figure 1**). The pair of images was captured from the illuminated sheet of fluorescent particles generated by a 25-mJ, double-pulsed Nd:YAG laser with the pulse separation of 1 ms.

The length of each pressure drop cycle was set to 100 ms, as mentioned earlier. The CCD camera used for DPIV took two pairs of images in each cycle. There were 20 consecutive cycles that were identical because of the same pressure drop ($\tau = 35 \pm 5$) applied. DPIV data were phase-averaged over the 20 identical cycles. Therefore, a total of 40 velocity/vorticity fields were captured for different time points of the rapid filling phase. This temporal resolution gave us an accurate estimate of the velocity and the vorticity fields to compute circulation of the vortex ring and to validate the exit jet velocity (U_J) obtained from different methods (equation 3). The CCD camera was triggered simultaneously with the first cycle of experiment and was synchronized with the PHOTRON high-speed cameras. The laser sheet was set perpendicular to the jet and cut through the center of the annulus. This configuration allowed analysis of velocity and vorticity fields resulting from the starting jet at the illuminated cross section.

Vortex ring circulation within its formation stages was computed from DPIV data (**Figure 2**). Based on saturation status of circulation, the onset of pinch-off was determined. Circulation (Γ) was computed from the vorticity field resulted from the velocity vector field. Vorticity (ω) is defined as the curl of the velocity vector:

$$\omega = \nabla \times \mathbf{u} \quad (6)$$

Circulation (Γ) is characterized as the line integral of the velocity. Based on the Stokes' theorem, the circulation around a reducible curve (c) is equal to the flux of vorticity through an open surface (Λ) with unit normal vector \mathbf{n} bounded by the curve, that is:

$$\Gamma = \oint_c \mathbf{u} \cdot d\mathbf{k} = \iint_{\Lambda} \omega \cdot \mathbf{n} ds \quad (7)$$

where the right side is a surface integral and the left side is a line integral; \mathbf{u} is the velocity vector,²⁸ ds is the surface element, and $d\mathbf{k}$ is the line element.

Control Volume Analysis

The momentum equation related to the setup was derived by considering the control volume (Ω) equations for the fluid inside the atrial tube (**Figure 3**). Flow was considered inertia dominant because of high Reynolds number at the annulus. Therefore, shear stress contribution to the momentum equation was neglected. Assuming constant gravitational field (\mathbf{g}) acting on the control volume (Ω) with moving boundary, the momentum equation would be described as:

$$\frac{\partial}{\partial t}(m\mathbf{U}_p) + \rho \int_{\partial\Omega} \mathbf{U}_J((\mathbf{U}_J - \mathbf{U}_p) \cdot \mathbf{n}) ds = m\mathbf{g} + \int_{\partial\Omega} (P_\infty - P) \mathbf{n} ds \quad (8)$$

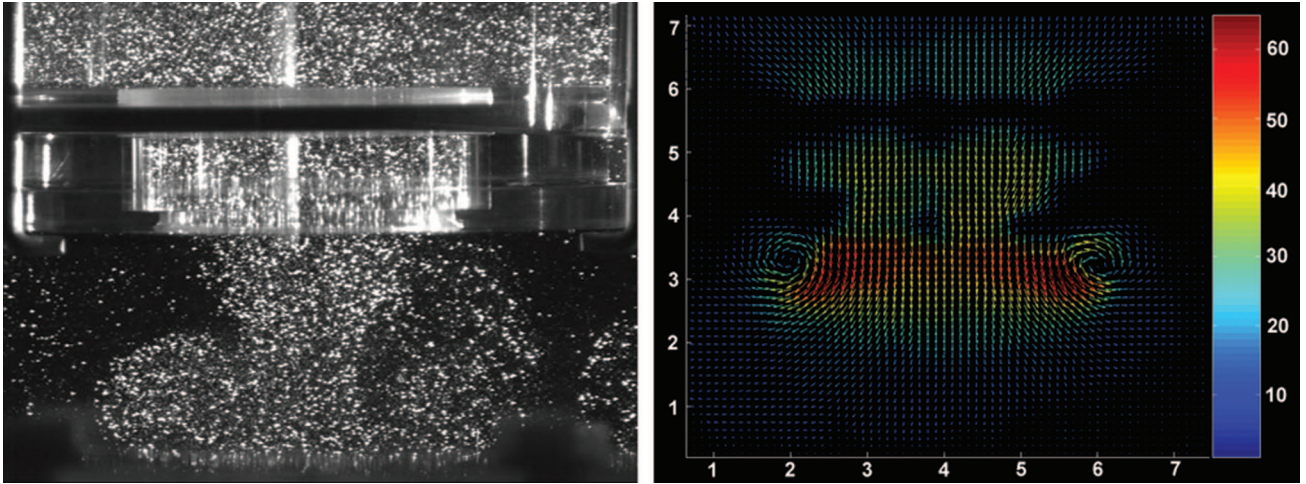


Figure 2. Left, Particle field of the experiment with $D_j = 3.00$ cm when a vortex ring is forming from transannulus flow. Right, Velocity field of the same experiment. The circulation (Γ) of the leading vortex ring was computed from a sequence of velocity fields.

where \mathbf{U}_j is the instantaneous exit jet velocity vector, \mathbf{U}_p is the annulus plane velocity vector, and m is the mass of the annulus plane, together with the instantaneous mass of the fluid:

$$m(t) = M_{Annulus} + \rho \int_{\Omega} dV_{\Lambda}(t) \quad (9)$$

P is the pressure at the annulus and P_{∞} is the pressure at the atrial side of the nozzle (Table 1). Based on the momentum, Equation 8, recoil force is described as:

$$\mathbf{F}_{recoil} = \frac{\partial}{\partial t} (m\mathbf{U}_p) = M_{Annulus}\mathbf{a}_p + \rho \int_{\Omega} \mathbf{a}_p dV_{\Lambda} + \rho \frac{\partial}{\partial t} \int_{\Omega} \mathbf{U}_p dV_{\Lambda} \quad (10)$$

where \mathbf{a}_p is the annulus plane acceleration vector. Thrust generated by the propulsion is described from the momentum equation as:

$$\mathbf{F}_{thrust} = \rho \int_{\partial\Omega} \mathbf{U}_j((\mathbf{U}_j - \mathbf{U}_p) \cdot \mathbf{n}) ds + \int_{\partial\Omega} (P - P_{\infty}) \mathbf{n} ds \quad (11)$$

This study considered uniform profile for the flow over the

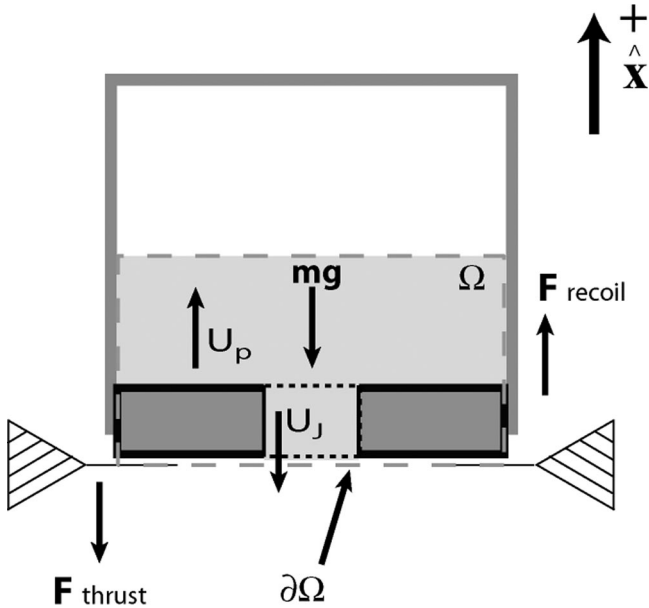


Figure 3. Embedded control volume (Ω) of fluid inside the atrial tube and at the annulus. \mathbf{U}_j is instantaneous exit jet velocity, \mathbf{U}_p is annulus plane velocity, \mathbf{F}_{thrust} is force generated by thrust, \mathbf{F}_{recoil} is recoil force exerted on the annulus plane, and $m\mathbf{g}$ is the weight of annulus plane plus instantaneous weight of water inside the atrial tube (over the annulus plane).

Table 1. Abbreviations and Acronyms

P	Trans-annulus pressure
P_0	Initial ventricular pressure
P_{LV}	Ventricular pressure
P_{∞}	Pressure at atrial side of the nozzle
τ	Pressure drop time-constant
V	Volume of fluid passes the annulus
U_j	Instantaneous exit jet velocity
U_A	Water-level velocity at the atrium
U_p	Annulus-plane velocity
u_{Piston}	Piston velocity
D_j	Annulus diameter
D_A	Atrial tube diameter
ρ	Water density
V_A	Volume of fluid in atrium
V_0	Initial volume of fluid in atrium
x_0	Initial position of water level in atrium
x	Instantaneous position of water-level
T^*	Formation time
t	Time
m	Mass of the annulus plane plus the atrial fluid
g	Gravitational acceleration
\mathbf{a}_p	Annulus plane acceleration
$M_{Annulus}$	Mass of the annulus plane
L_A	Ejecting height of water-level at atrium
L_j	Nominal ejected jet length
Γ	Circulation
ω	Vorticity

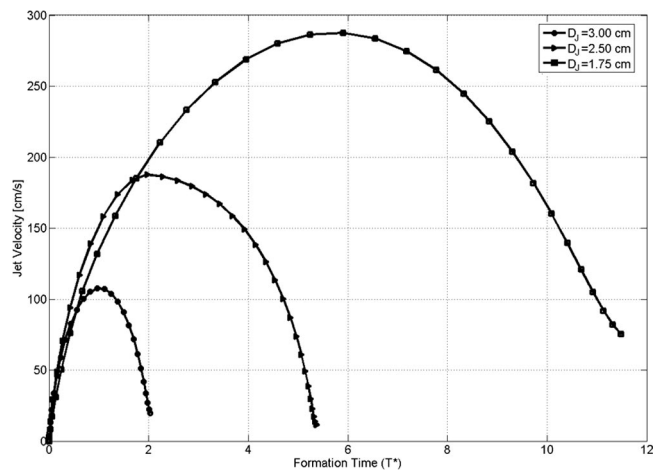


Figure 4. Exit jet velocity for each annulus diameter as a function of formation time. For the largest annulus size case ($D_J = 3.00$ cm), velocity reached its maximum (108 ± 8 cm/s) at $T^* = 0.97 \pm 0.3$ and the transannulus flow completed at around $T^* = 2.0$. For $D_J = 2.50$ cm, transannulus jet reached its peak velocity (188 ± 10 cm/s) at $T^* = 2 \pm 0.2$ and the flow ended before $T^* = 6$. By using the smallest annulus size ($D_J = 1.75$ cm), transannulus jet velocity reached its maximum (287 ± 11 cm/s) at $T^* = 5.90 \pm 0.6$ and the flow terminated around $T^* = 12.00$.

annulus. The only external force that applied to the surface of control volume was the weight of annulus plane together with the fluid at each instant of time. Considering the direction of forces (**Figure 3**), Equations 8, 10, and 11 are summarized as:

$$\mathbf{F}_{\text{recoil}} - \mathbf{F}_{\text{thrust}} = m\mathbf{g} \quad (12)$$

Results

Exit Jet Velocity and Formation Time

Exit jet velocity for each annulus diameter was computed on the basis of Equation 3 (**Figure 4**). Formation time was computed on the basis of the instantaneous exit jet velocity (equation 3) and the corresponding annulus diameter. For comparison purposes, all the results were shown as a function of formation time, which is a nondimensional time parameter.³ For the largest annulus size ($D_J = 3.00$ cm), velocity reached its maximum (108 ± 8 cm/s) at $T^* = 0.97 \pm 0.3$, and the transannulus flow ended at around $T^* = 2.00$. For $D_J = 2.50$ cm, the transannulus jet reached its peak velocity (188 ± 10 cm/s) at $T^* = 2.00 \pm 0.2$, and the flow ended before $T^* = 6.00$. By using the smallest annulus size ($D_J = 1.75$ cm), transannulus jet velocity reached its maximum (287 ± 11 cm/s) at $T^* = 5.90 \pm 0.6$, and the flow terminated around $T^* = 12.00$ (**Figure 4**).

Transannulus Pressure

Transannulus pressure (P) was measured as the pressure difference between the atrial tube and the ventricular chamber at the annulus level. The transannulus pressure normalized with the initial LV pressure (P_0) for each case plotted as function of formation time (**Figure 5**). For $D_J = 3.00$ cm, pressure at the annulus dropped to 20% of its initial value at $T^* = 1.10 \pm 0.2$. The same extent of pressure drop occurred for $D_J = 2.50$

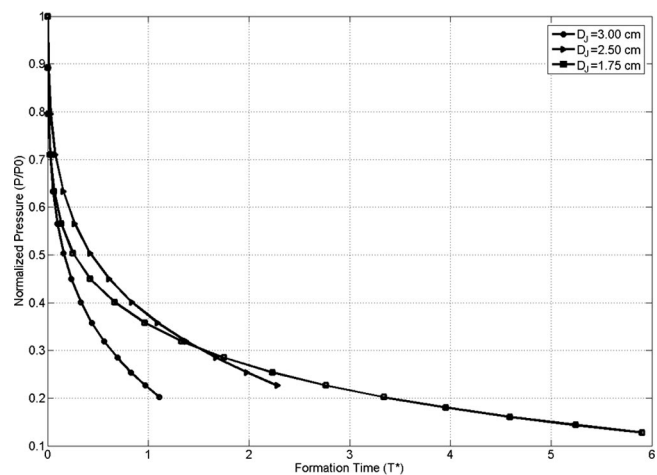


Figure 5. Transannulus pressure normalized with initial LV pressure (P_0). For $D_J = 3.00$ cm, pressure at the annulus dropped to 20% of its initial value at $T^* = 1.10 \pm 0.2$. For $D_J = 2.50$ cm, pressure at the annulus dropped to 20% of its initial value at $T^* = 2.30 \pm 0.3$. For $D_J = 1.75$ cm, pressure at the annulus dropped to 20% of its initial value at $T^* = 3.40 \pm 0.3$.

cm at $T^* = 2.30 \pm 0.3$ and for $D_J = 1.75$ cm at $T^* = 3.40 \pm 0.3$.

Recoil Force and Thrust

For each annulus size, the velocity (\mathbf{U}_p) and the acceleration of the annulus plane (a_p) were measured, and the recoil force ($\mathbf{F}_{\text{recoil}}$) was computed on the basis of momentum (Equation 8). The recoil force as a function of formation time is shown in **Figure 6** for each annulus size. For $D_J = 3.00$ cm, recoil force reached its peak at $T^* = 2.00 \pm 0.1$; for $D_J = 2.50$ cm, the maximal recoil force was attained at $T^* = 3.8 \pm 0.2$, and for $D_J = 1.75$ cm, the force had the peak at $T^* = 11.00 \pm 0.4$ (**Figure 6**).

Force generated by thrust (F_{thrust}) was computed on the basis

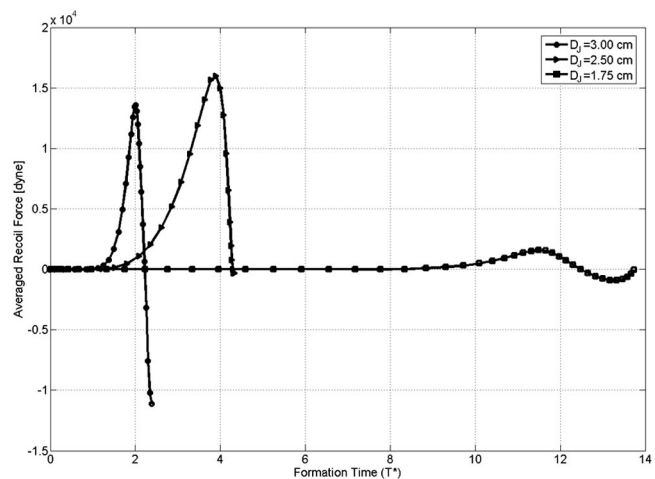


Figure 6. Time-averaged recoil force for the considered cases. For $D_J = 3.00$ cm, recoil force reached its peak at $T^* = 2.00 \pm 0.1$, for $D_J = 2.50$ cm, the maximal recoil force was attained at $T^* = 3.8 \pm 0.2$, and for $D_J = 1.75$ cm, the force had the peak at $T^* = 11.00 \pm 0.4$.

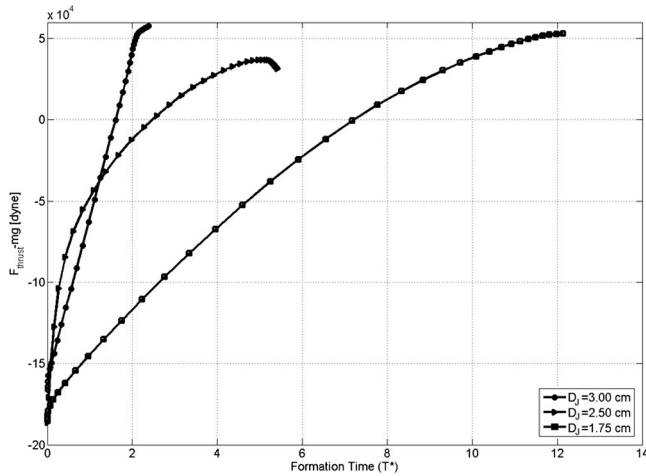


Figure 7. Time-averaged thrust subtracted by the instantaneous weight of the water column in atrium. For $D_j = 3.00$ cm, thrust reached its peak at $T^* = 2.00 \pm 0.1$, for $D_j = 2.50$ cm, the maximal thrust was attained at $T^* = 5.0 \pm 0.4$, and for $D_j = 1.75$ cm, the forced had the peak at $T^* = 11.00 \pm 0.3$.

of exit jet velocity, annulus plane velocity, and pressure at the annulus.¹¹ The magnitude of thrust can be compared with the recoil force in **Figures 6** and **7**. The thrust subtracted by instant weight of the atrial tube (mg) versus formation time is shown in **Figure 7** for each annulus size. For $D_j = 3.00$ cm, thrust reached its peak at $T^* = 2.00 \pm 0.1$; for $D_j = 2.50$ cm, the maximal thrust was attained at $T^* = 5.0 \pm 0.4$, and for $D_j = 1.75$ cm, the forced had the peak at $T^* = 11.00 \pm 0.3$ (**Figure 7**).

The recoil force was computed on the basis of Equation 10 by tracking the annulus movement and transannulus flow with the high-speed camera. Likewise, the thrust magnitude was computed by measuring variations in transannulus pressure together with the instantaneous jet velocity (Equation 11).

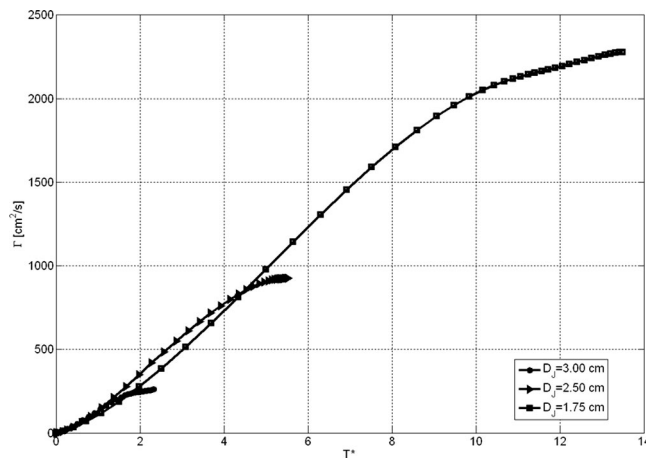


Figure 8. Circulation of the ejected vortex ring obtained from vorticity/velocity fields versus formation time for each annulus diameter. The slope of circulation curve dramatically flattens at $T^* = 2.00 \pm 0.2$ for $D_j = 3.00$ cm. For $D_j = 2.50$ cm, the circulation curve starts to saturate at $T^* = 4.00 \pm 0.2$, and for $D_j = 1.75$ cm, the circulation curve grew until $T^* = 13.00 \pm 0.6$, at which the circulation curve began to flatten.

Considering that F_{recoil} and F_{thrust} were computed from different experimental techniques, the slight discrepancies in the relative timings of the two quantities could be attributed to measurement errors.

Circulation

Circulation of the ejected vortex ring was computed on the basis of vorticity/velocity fields (Equations 6 and 7) obtained from phase-averaged DPIV (**Figure 8**). The vortex ring pinches off when no additional energy or circulation is added to the leading vortex ring.³ By plotting the circulation versus formation time, the incident of pinch-off (formation number) can be defined as the formation time (T^*) at which the circulation curve saturates. **Figure 9** compares the vortex ring circulation as a function of formation time for each annulus diameter studied. It can be observed that the slope of the circulation curve dramatically flattens at $T^* = 2.00 \pm 0.2$ for $D_j = 3.00$ cm. For $D_j = 2.50$ cm, the circulation curve starts to saturate at $T^* = 4.00 \pm 0.2$. However, for $D_j = 1.75$ cm, the circulation curve grows further than the former cases until $T^* = 13.00 \pm 0.6$, at which the circulation curve began to flatten (**Figure 8**).

Discussion

The timing of transannulus pressure drop was found to be inversely correlated with the size of the annulus, regardless of the similar pressure drop ($\tau = 35 \pm 5$) in ventricular chamber (**Figure 5**). Faster pressure drop for $D_j = 3.00$ cm resulted in completion of transannulus flow (volume transfer) in a shorter formation time (**Figure 3**). For $D_j = 2.50$ cm and $D_j = 1.75$ cm, transannulus flow completed in $T^* = 5.40 \pm 0.5$ and $T^* = 11.30 \pm 0.6$, respectively.

Although the volume of fluid transferred between two chambers were identical, the magnitude and the instant of the recoil force was not the same for the annulus diameters studied (**Figure 6**). Therefore, the size of the annulus is a significant parameter in the dynamics of the annulus plane during transannulus flow. This study was designed in such a way that no forces other than the ones generated by the transannulus flow can affect the annulus plane. As a matter of fact, we computed the thrust generated during propulsion (**Figure 7**) and the circulation of the ejected vortex ring for each case (**Figure 8**) to correlate with the annulus plane recoil force.

The final magnitude of thrust generated by each annulus diameter was almost identical, whereas the time taken for each annulus to reach the peak thrust was different (**Figure 7**). This was the consequence of how momentum transferred from one chamber to another, and the peak incident showed a direct relation with the period needed to complete the volume transfer (**Figures 4** and **7**). Considering the recoil force (**Figure 6**), it can be observed that it reached a peak (**Figure 6**) once the thrust force was close to its maximal magnitude (**Figure 7**), thus confirming the same occurrence of the recoil force and the thrust.

The other parameter that was found to be changing with different annulus sizes was the vortex ring circulation (**Figure 8**). It has been observed that decreasing the size of the annulus increases the final magnitude of the circulation (**Figure 8**). However, the formation time at which the magnitude of the circulation saturated was different for each annulus size. The

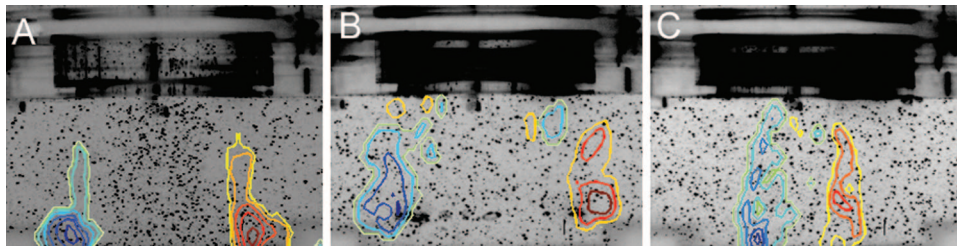


Figure 9. Snapshot of the vorticity field obtained by DPIV for different cases at the onset of peak recoil force. (A) $D_j = 3.00$ cm: In this case, the vorticity field shows that the leading vortex was not yet pinched off ($T^* = 2.00 \pm 0.1$), whereas it was hitting the bottom wall. This prevented further growth of the leading vortex ring. (B) $D_j = 2.50$ cm: In this case, the leading vortex has just pinched off ($T^* = 3.8 \pm 0.2$). (C) $D_j = 1.75$ cm: In this case, the recoil force had a peak at $T^* = 11.00 \pm 0.4$. The corresponding vorticity field shows that there was only a trailing jet, meaning that the leading vortex ring had already been pinched off.

larger the annulus diameter, the sooner the circulation saturates.

Considering the trend of vortex ring circulation and the incident of maximal recoil force (**Figures 6 and 8**) for $D_j = 3.00$ cm and $D_j = 2.50$ cm, it can be observed that the peak recoil force occurred at the formation time ($T^* = 2.00 \pm 0.1$ and $T^* = 3.8 \pm 0.2$, respectively) in which circulation was saturating ($T^* = 2.00 \pm 0.2$ and $T^* = 4.00 \pm 0.2$, respectively). For the case $D_j = 1.75$ cm, the peak recoil force occurred at $T^* = 11.30 \pm 0.3$, later than the formation time at which circulation saturated ($T^* = 10.00 \pm 0.3$).

It has been shown before that a vortex ring is considered pinched off when the circulation does not increase, which means that the leading vortex ring does not receive any additional energy from the starting jet.⁴ In the present study, it was found that for $D_j = 3.00$ cm and $D_j = 2.50$ cm, both maximal recoil force and maximal jet thrust occurred at the formation time in which vortex ring circulation was saturated. **Figure 9** shows a snapshot of the vorticity field obtained by phase-averaged DPIV for each case at the onset of peak recoil force. The maximal value of the recoil force was attained in the case with $D_j = 2.50$ cm at $T^* = 3.8 \pm 0.2$. In this case, the formation time at which the recoil-force peak occurred was in the range of the formation number defined by Gharib *et al.* This implies that all the circulation produced in the pulsed jet went into the leading vortex ring, thereby maximizing the recoil force. This was also confirmed by the vorticity plot in **Figure 9B**, which shows that the leading vortex pinches off at this formation time.

For the largest annulus ($D_j = 3.00$ cm), the recoil force had a peak at $T^* = 2.00 \pm 0.1$. However, the peak recoil force was smaller than the medium-sized annulus ($D_j = 2.50$ cm). The vorticity field in **Figure 9A** shows that at this formation time, the leading vortex was not yet pinched off, whereas it was hitting the bottom wall. This prevented the further growth of the leading vortex ring, thereby limiting the corresponding recoil force and further increase in magnitude of circulation (**Figure 8**). For the smallest annulus ($D_j = 1.75$ cm), the recoil force had a peak at $T^* = 11.30 \pm 0.3$, and the peak value was the smallest among all the three annulus sizes. By comparing **Figures 6 and 8**, it can be inferred that at the incident of recoil force ($T^* = 11.30 \pm 0.3$), the circulation curve has been flattened earlier and thus the vortex ring was already pinched off ($T^* = 10.00 \pm 0.3$). This assumption was also confirmed by the corresponding vorticity field at the onset of peak recoil force

plotted in **Figure 9C**. In this case, it was apparent that the vortex ring has already hit the bottom before and the vorticity is no longer entrained from the shear layer region of the trailing jet. The recoil force in this case was the result of the trailing jet rather than the consequence of vortex ring pinch-off, and that might be a reason for its much smaller magnitude compared with the other two annulus sizes (**Figure 6**).

Equivalent Piston-Cylinder Setup

Starting jets are typically created by using piston-cylinder setup. To relate the results of the present study to the other known results for a standard piston-cylinder setup, an equivalent stroke ratio (SR) was defined for each annulus size as the ratio of the length of jet (L_j) to the jet diameter (D_j). These quantities were obtained on the basis of conservation of mass and equating volumes of fluid exchanged between the two chambers:

$$V_{ejected} = \frac{\pi}{4} D_A^2 \cdot L_A = \frac{\pi}{4} D_j^2 \cdot L_j \quad (13)$$

where $V_{ejected}$ is the total volume of fluid ejected from atrial tube in a single run, L_A is the water level height change in the atrial tube ($L_A = 1.00$ cm; constant for all the cases), and L_j is the nominal jet length or the distance traveled by a piston with diameter D_j ejecting the same volume from an equivalent piston-cylinder setup. In other words, if the total ejected volume is kept constant, the equivalent SR can be attributed to an equivalent experiment performed with a piston-cylinder setup in which the total volume of ejected fluid is the same.

Based on Equation 13, the equivalent stroke ratios were 9.14 for $D_j = 1.75$ cm, 3.12 for $D_j = 2.50$ cm, and 1.80 for $D_j = 3.00$ cm. The equivalent piston-cylinder setup that generated the maximal recoil force (**Figure 6**) had an SR of 3.12, which, among all cases, was the closest one to the ratio that Krueger and Gharib¹³ found to generate maximal averaged thrust. It was also found that the recoil force was maximized at a formation time close to the equivalent SR for each case (**Figure 6**). This was expected because the total thrust for the three cases was conserved (**Figure 7**) due to the constant ejected volume.¹³ However, the magnitude of the peak recoil force was different in each case (**Figure 6**).

Physiologic Significance

It has been shown previously that the normal pattern of LV filling would be altered because of the diastolic dysfunction, which occurs during the development of heart failure.^{29–31} This variation in transmitral flow would also be reflected in diastolic motion of the mitral annulus measured by Doppler tissue imaging (DTI).³² DTI of the mitral annulus has been recognized as an effective indicator of LV function in human heart.^{33,34} The peak velocity of the mitral annulus away from the apex during early diastole (E_M), indicating the rate of longitudinal expansion of the LV, is reduced in patients with impaired diastolic relaxation.³⁵

In the present study, we showed that in a simplified model of the left heart, the variation in jet stroke ratio can be reflected in the dynamics of the mitral annulus plane. More specifically, we found that for a physiologic base-apex distance and an annulus diameter of 2.50 cm, which closely approximates the normal annulus diameter in adults, if the physiologic pressure decay applied, the annulus plane recoil force would be maximal at the time in which the vortex ring pinches off. In a real heart, the complex geometry and the viscoelastic properties of the ventricular chamber as well as the wall-flow interaction and viscosity are also responsible for variations in dynamics of mitral annulus. However, the above-mentioned parameters directly influence transmitral flow and the formed vortex ring.

Almost all the patients with idiopathic dilated cardiomyopathy have a significantly large mitral annulus.³⁶ Therefore, as a result the transmitral jet, stroke ratio would be different from a normal LV. In a recent study, Mori *et al.*³⁷ showed that the peak mitral annulus velocity also would be lower than normal in cases with dilated cardiomyopathy. The results of their study is congruent with our observation, confirming that by increasing the annulus diameter more than 2.50 cm, even if a physiologic LV pressure drop is applied, the annulus recoil is not optimum when compared with normal.

On the other hand, another recent study³⁸ has demonstrated that the LV long-axis function, evaluated by DTI in patients with pure mitral stenosis, is significantly impaired despite the normal global systolic function. In this case, if the LV pressure drop during diastole remains constant, the transmitral jet stroke ratio will increase. This observation is also consistent with our study corroborating that by decreasing the mitral annulus diameter, despite the fact that the transmitral jet velocity increases, the annulus recoil force will be smaller than the normal case.

Conclusion

The present *in vitro* study confirms the presence of a vortex ring during rapid filling phase of diastole and implies that the process of vortex ring formation can influence mitral annulus dynamics. Additionally, this study suggests that vortex ring formation can be used as an index for assessment of LV function during diastole and as a factor that should be considered in design and implementing cardiac prosthetics devices.

Limitations

In this study, we did not consider the active myocardial contractions, interaction of valve leaflet and flow, and the

blood viscosity on formation of the vortex ring. Works are in progress to design and use an actively contracting chamber for mimicking cardiac expansion, using Bioprosthetic heart valves in mitral position and blood analogs for viscose flow. Another limitation of this study was using a phase-averaged DPIV technique, which slightly increased the error because of the fast nature of the experiment. Works are in progress to use continuous laser for illumination and high-speed cameras for stereo-PIV to obtain more accurate results.

Acknowledgments

The authors are grateful to Prof. Anthony Leonard for the useful discussions on control volume analysis and to Prof. Michael Dickinson and his group for using their high-speed cameras.

References

1. Didden N: On the formation of vortex rings: rolling-up and production of circulation. *Z Angew Math Phys* 30: 101, 1979.
2. Shariff K, Leonard A: Vortex rings. *Annu Rev Fluid Mech* 24: 235, 1992.
3. Gharib M, Rambod E, Shariff K: A universal time scale for vortex ring formation. *J Fluid Mech* 360: 121–140, 1998.
4. Rosenfeld M, Rambod E, Gharib M: Circulation and formation number of laminar vortex rings. *Fluid Mech* 376: 297–318, 1998.
5. Bellhouse BJ: Fluid mechanics of a model mitral valve and left ventricle. *Cardiovasc Res* 6: 199–210, 1972.
6. Reul H, Talukder N, Muller W: Fluid mechanics of the natural mitral valve. *J Biomech* 14: 361–372, 1981.
7. Kim WY, Bisgaard T, Nielsen SL, *et al*: Two-dimensional mitral flow velocity profiles in pig models using epicardial echo Doppler Cardiography. *J Am Coll Cardiol* 24: 532–545, 1994.
8. Vierendeels JA, Dick E, Verdonck PR: Hydrodynamics of color M-mode Doppler flow wave propagation velocity $V(p)$: a computer study. *J Am Soc Echocardiogr* 15: 219–224, 2002.
9. Kim WY, Walker PG, Pedersen EM, *et al*: Left ventricular blood flow patterns in normal subjects: a quantitative analysis by three dimensional magnetic resonance velocity mapping. *J Am Coll Cardiol* 26: 224–238, 1995.
10. Kilner PJ, Yang GZ, Wilkes AJ, *et al*: Asymmetric redirection of flow through the heart. *Nature* 404: 759–761, 2000.
11. Johari H, Rixon GS: Effects of pulsing on a vortex generator jet. *AIAA J* 41: 2309–2315, 2003.
12. Cater JE, Soria J: The evolution of round zero-net-mass-flux jets. *J Fluid Mech* 472: 167–200, 2002.
13. Krueger PS, Gharib M: The significance of vortex ring formation to the impulse and thrust of a starting jet. *Physics Fluids* 15: 1271–1281, 2003.
14. Steen T, Steen S: Filling of a model left ventricle studied by colour M mode Doppler. *Cardiovasc Res* 28: 1821–1827, 1994.
15. Baccani B, Domenichini F, Pedrizzetti G, Tonti G: Fluid dynamics of the left ventricular filling in dilated cardiomyopathy. *J Biomech* 35: 665–671, 2002.
16. Weiss JL, Fredriksen JW, Weisfeldt ML: Hemodynamic determinants of the time course of fall in canine left ventricular pressure. *J Clin Invest* 58: 751–760, 1976.
17. Yellin EL, Nikolic S, Frater RWM: Left-ventricular filling dynamics and diastolic function. *Prog Cardiovasc Dis* 32: 247–271, 1990.
18. Yellin EL, Hori M, Yoran C, *et al*: Left-ventricular relaxation in the filling and nonfilling intact canine heart. *Am J Cardiol* 250: H620–H629, 1986.
19. Rodriguez F, Langer F, Harrington KB, *et al*: Importance of mitral valve second-order chordae for left ventricular geometry, wall thickening mechanics, and global systolic function. *Circulation* 110: II-115–II-122, 2004.
20. Standring S: *Gray's Anatomy: The Anatomical Basis of Clinical Practice*. Oxford: Churchill Livingstone; 39th ed, 2004.
21. Dong SJ, Hees PS, Siu CO, *et al*: MRI assessment of LV relaxation by untwisting rate: a new isovolumic phase measure of t. *Am J Physiol Heart Circ Physiol* 281: H2002–H2009, 2001.
22. Ommen SR, Nishimura RA, Appleton CP, *et al*: Clinical utility of

- Doppler echocardiography and tissue Doppler imaging in the estimation of left ventricular filling pressures: a comparative simultaneous Doppler-catheterization study. *Circulation* 102: 1788–1794, 2000.
23. Guyton AC, Hall JE. *Textbook of Medical Physiology*. 10th ed, Philadelphia, PA: WB Saunders Company, 2000.
 24. Brutsaert DL, Rademakers FE, Sys SU: Triple control of relaxation: implications in cardiac disease. *Circulation* 69: 190–196, 1984.
 25. Brutsaert DL, Sys SU: Relaxation and diastole of the heart. *Physiol Rev* 69: 1228–1315, 1989.
 26. Gilbert JC, Glantz SA: Determinants of left ventricular filling and of the diastolic pressure/volume-relationship. *Circ Res* 64: 827–852, 1989.
 27. Willert CE, Gharib M: Digital particle image velocimetry. *Exp Fluids* 10: 181–193, 1991.
 28. Kheradvar A, Kasalko J, Johnson D, Gharib M: An in vitro study of changing profile heights in mitral bioprostheses and their influence on flow. *ASAIO J* 52: 34–38, 2005.
 29. Appleton CP: Doppler assessment of left ventricular diastolic function: the refinements continue. *J Am Coll Cardiol* 21: 1697–1700, 1993.
 30. Ohno M, Cheng CP, Little WC: Mechanism of altered patterns of left ventricular filling during the development of congestive heart failure. *Circulation* 89: 2241–2250, 1994.
 31. Nishimura RA, Tajik AJ: Evaluation of diastolic filling of left ventricle in health and disease: Doppler echocardiography is the clinician's Rosetta stone. *J Am Coll Cardiol* 30: 8–18, 1997.
 32. Nagueh SF: Noninvasive evaluation of hemodynamics by Doppler echocardiography. *Curr Opin Cardiol* 14: 217–224, 1999.
 33. Nagueh SF, Middleton KJ, Kopelen HA, et al: Doppler tissue imaging: a noninvasive technique for evaluation of left ventricular relaxation and estimation of filling pressures. *J Am Coll Cardiol* 30: 1527–1533, 1997.
 34. Sanderson JE, Wang M, Yu CM: Tissue Doppler imaging for predicting outcome in patients with cardiovascular disease. *Curr Opin Cardiol* 19: 458–463, 2004.
 35. Hasegawa H, Little WC, Ohno M, et al: Diastolic mitral annular velocity during the development of heart failure. *J Am Coll Cardiol* 41: 1590–1597, 2003.
 36. Kwan J, Shiota T, Agler DA, et al: Geometric differences of the mitral apparatus between ischemic and dilated cardiomyopathy with significant mitral regurgitation: real-time three-dimensional echocardiography study. *Circulation* 107: 1135–1140, 2003.
 37. Mori K, Edagawa T, Inoue M, et al: Peak negative myocardial velocity gradient and wall-thickening velocity during early diastole are noninvasive parameters of left ventricular diastolic function in patients with Duchenne's progressive muscular dystrophy. *J Am Soc Echocardiogr* 17: 322–329, 2004.
 38. Ozer N, Can I, Atalar E, et al: Left ventricular long-axis function is reduced in patients with rheumatic mitral stenosis. *Echocardiography* 21: 107–112, 2004.